Disentangling the normal aging from the pathological Alzheimer's disease progression on cross-sectional structural MR images

Marco Lorenzi, Xavier Pennec, Nicholas Ayache, Giovanni Frisoni

Disentangling the Normal Aging from the Pathological Alzheimer's Disease Progression on Cross-sectional Structural MR Images.

Marco Lorenzi[1,2], Xavier Pennec[1], Nicholas Ayache[1], and Giovanni Frisoni[2] for the Alzheimer's Disease Neuroimaging Initiative [*]

[1] Project Team Asclepios, INRIA Sophia Antipolis, France

[2] LENITEM, IRCCS San Giovanni di Dio, Fatebenefratelli, Italy

Abstract. The morphology observed in the brain of patients affected by Alzheimer's disease (AD) is the contribution of different biological processes such as the normal aging and the AD-specific pathological matter loss. The ability to differentiate these complementary biological factors is fundamental in order to reliably evaluate the pathological AD-related structural changes, especially at the earliest phase of the disease, at prodromal and pre-clinical stages. We propose a method based on non rigid-registration to estimate the different contributions of these complementary factors, and to identify the brain structural changes which are specific for the pathological component. The experimental results provide a description of the anatomical changes observed across the AD time span: normal aging, normal aging at risk, conversion to MCI and latest AD stages. More advanced AD stages are associated to "virtually older" brains, and to increased specific morphological changes that are not related to the normal aging. These results provide new insights that can

---

lead to new understandings of the AD dynamics, and to novel techniques for the modeling and the early detection of the disease.

1   Introduction.

The objective of computational anatomy applied to neurodegenerative diseases such as Alzheimer's disease (AD) is the understanding of the pathological changes affecting the brain morphology. This is particularly relevant for monitoring the disease evolution in clinical trials and for diagnostic purposes [7,13].

However, the morphology of the brain affected by AD is not completely related to the disease, especially in asymptomatic and prodromal stages, and is the consequence of specific biological processes:

– *Age related anatomical changes.* It is well known that the healthy aging is characterized by the progressive deterioration of the brain structural integrity [9] which involves essentially hippocampal loss and ventricular enlargement.

– *Disease related anatomical changes.* AD involves a specific pathological process which was demonstrated to be complementary to the healthy aging [12,1], and to produce patterns of neurodegeneration in specific areas which cannot be ascribed to any kind of global accelerated aging process [7].

If we could independently model these physiological changes it would then be possible to describe a given anatomy as the contribution of distinct and complementary factors, each of them representing a precise biological process. Such decomposition would be extremely interesting not only for the improvement of the understanding of the disease, by removing sources of variability not related to the pathology, but also for clinically oriented purposes, such as the early diagnosis and the development of drugs aimed to target the disease specific component.

However, such a decomposition comes with a number of issues that must be dealt with. For instance, it is important to notice that, although induced by completely different biological mechanisms, aging and AD often map to common areas, and the correct identification of the respective contributions may be difficult, especially in morphometric studies. Moreover it is plausible that these phenomena are not completely independent, and might interact in a kind of positive "feedback" process. Thus, the increase of the specific changes leads to an accelerated global aging process in the long term. This hypothesis is supported by recent studies on the estimation of aging indices based on the structural MRI of the brain [6,4]. For instance, in [6] the authors showed a strong correlation between the predicted age and the biological one, but estimated a gap of +10 years for subjects with AD.

The reliable estimation of the aging component is also relevant for modeling the evolution of the disease and for the subsequent statistical analysis. For example, when comparing the longitudinal observations from different clinical groups at different aging stages it is crucial to correctly position the observations on the time axis. This is not an evident task, since the disease appears at different ages, and biologically older brains might have greater structural integrity than younger ones affected by the pathology. For this purpose it is very important to define a"virtual" aging stage relative to a reference anatomical evolution.

The objective of this work is to introduce a framework for the identification and the disentanglement of the biological processes due to aging and pathological changes. In particular, by following the model which relates the development of AD to the abnormal processing of beta-amyloid ($A\beta$) peptide [8], we investigate the atrophy patterns in healthy subjects positive to the CSF $A\beta42$ marker, in MCI converters to AD, and finally in AD. The method is based on the diffeomorphic non rigid-registration and is detailed in Section 2. In Section 3 we show

that such framework provides an accurate description of the anatomical changes across the AD stages, which can find effective applications in the modeling of the disease and for diagnostic purposes.

2   Methods.

Given a subject k, we model the brain anatomy I_k observed in a magnetic resonance image (MRI) by non-rigid registration to a pre-defined reference anatomical space T. If we parameterize the subject-to-template deformation ϕ_k by a stationary velocity fields (SVFs) w_k such that $\phi_k = \exp(w_k)$, the observed anatomical structure is then described by the SVF w_k, which is a tangent vector field in the deformation space.

By taking advantage of the log-Euclidean nature of the SVF, we assume that w_k is the contribution of the normal aging plus a complementary component: $w_k = w_{age}^k + w_{specific}^k$.
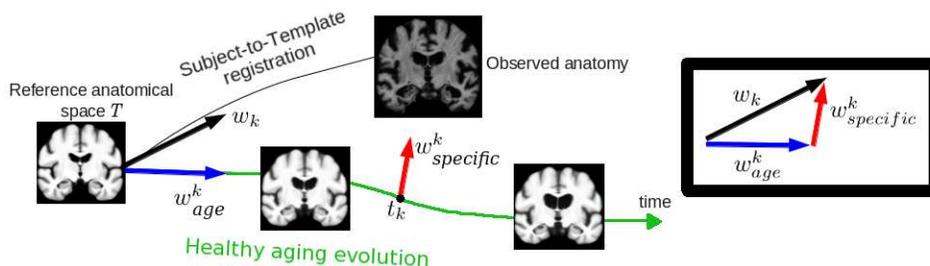

Fig. 1: An observed anatomy can be described in terms of an aging factor plus a subject specific component not related to the healthy aging.

The proposed framework analyzes these different components by describing the observed anatomy in separate modeling steps which respectively address:

1. Identification and extraction of the aging component w_{age} by estimation of a "virtual age" with respect to a reference evolution for the normal aging.

2. Identification and analysis of the remaining specific component $w_{specific}$. The specific component describes the cross-sectional changes which cannot be attributed to the aging, and which encode the pathological atrophy.

Each modeling step is separately addressed in the following sections.

2.1 Identification and Extraction of the Aging Component.

The "Virtual Age" with Respect to a Model of Healthy Aging. We want to differentiate the morphological patterns in the image I_k due to the normal aging from those related to different biological processes.

We consider a model of the healthy aging defined in a reference anatomical space T. As proposed in [10] we assume that the aging process is stationary and linearly evolving according to the SVF μ_0, so that the aging is defined as the trajectory $\mu(t) = t\mu_0$.

Theoretically, given a longitudinal evolution $\exp(\mu(t))$ for the healthy aging in a reference anatomy T, we want to project the subject's anatomy I_k on the "closest" point of the trajectory $T \circ \exp(\mu(t))$ in order to determine its progression stage t_k with respect to the evolution. Defining $\exp(w_k)$ as the subject-to-template deformation, and given a metric $<,>$ on the tangent space, the projection of the image I_k in the trajectory $T \circ \exp(\mu)$ is given by the decomposition of the vector into orthogonal components $w_k = w_{age}^k + w_{specific}^k = t_k\mu_0 + \nu_k$. In the present work the projection is based on the standard L^2 metric.

In such decomposition the time point t_k defines a "virtual age" index of the subject k with respect to the model μ, while the vector field ν_k encodes the morphological changes which cannot be related to the aging process (Figure 1). The time point t_k defines the projection on the longitudinal evolution $\mu(t)$

and is given by the whole brain average of the voxel-by-voxel (L^2) projections: $t_k = \frac{<w_k, \mu_0>_{(x)}}{||\mu_0||^2_{(x)}}$. Once t_k is determined, the specific vector component is simply computed voxel-wise as $\nu_k = w_k - t_k\mu_0$.

By estimating the time point t_k on the whole brain we make a precise assumption on the aging process, which is here defined *globally*. Therefore, the accelerated aging is constrained with respect to the model $t\mu_0$, and any local departure from it (for instance in some specific regions), is interpreted as a *specific* morphological change, independent from aging. On the contrary, by considering only regional projections on specific areas (for instance hippocampi or ventricles) we may mistake specific patterns of neurodegeneration as global accelerated aging, and thus introduce a bias in the decomposition.

2.2 Identification and Analysis of the Specific Component

The removal of the factor $t_k\mu_0$ allows to directly compare across subjects the remaining component $w^k_{specific} = \nu_k$, which encodes the variability that cannot be attributed to the normal aging. In this section, we investigate the ability of such component to correctly encode the information inherent the pathology, in order to reliably discriminate between different clinical populations.

Divergence Associated to the Specific Components. We are interested in the analysis of the specific *matter loss* which characterizes different clinical groups. The diffeomorphic constraint of the non-rigid registration encodes the morphological changes as a complementary compression/expansion process across adjacent areas. The compression models the shrinking of the anatomical structures due to the observed matter loss, while the expansion is a complementary process which indicates growth, for instance of the CSF areas in the ventricles or in the sulci surrounding the gray matter. These processes are induced by the estimated deformation fields and can be quantified by the flux of

the vectors across the boundary of the regions: the inward (resp. outward) flow across a surface induces the compression (resp. expansion) which quantifies the atrophy (resp. growth).

The compression/expansion processes are identified by the divergence $\nabla \cdot \nu_k$ associated to the vector component ν_k. We recall that from the Divergence (or Ostrogradsky's) theorem, the integral of the divergence of a vector field in a given region is the flux of the vector field across the boundaries of the region, and that the flux is the mathematical formulation of the boundary shift [11]. Since the regional divergence is the flux across regions, it measures the percentage matter loss.

Discriminative analysis on the specific component. In the present analysis we tested the ability of the divergence maps $\nabla \cdot \nu_k$ to discriminate between a set of patients P and a control group C.

We computed the voxel-by-voxel effect size map for the group-wise divergence $ES = (mean(\nabla \cdot \nu_P) - mean(\nabla \cdot \nu_C))/sd(\nabla \cdot \nu_P)$ which quantifies the magnitude of the differences between patients and control populations. We chose a set of regions relevant for AD (hippocampi, medial temporal lobes (MTL), posterior cingulate (PC), and ventricles) where we identified the voxels of maximal positive and negative effect size. These voxels were then inflated and symmetrized in order to define a set of regions for the discriminative analysis (Fisher's discriminant analysis) of the flux associated to the specific component. The discriminative analysis was performed by leave-one-out cross validation to test the correct group classification.

3 Experiments

We chose the ADNI structural MRIs for 57 healthy subjects with normal levels of CSF Aβ42 ($>$ 192 pg/ml, group Aβ-), 41 healthy subjects with abnormal levels (group Aβ+), 86 subjects with mild cognitive impairment who consequently converted to AD (group MCI_{conv}), 110 MCI subjects who remained stable during the observation period (group MCI_{stable}), and 134 AD patients (group AD). Demographical as well clinical information are based on the ADNI data updated to March 2012, with a follow-up period of 3 years from baseline.

Previous studies showed that healthy elders with pathological CSF Aβ42 levels ($> 192 pg/ml$) have a more pronounced brain atrophy progression [10,5,14], which might be a marker of pre-symptomatic stage of AD. Therefore we defined the healthy aging progression by considering only the Aβ- group as reference healthy population. The longitudinal observations (from baseline to 3 years) for the Aβ- group were used to model the reference healthy evolution μ_0 [10] normalized to an anatomical reference T estimated from the ADNI healthy population.

In order to unbias the analysis with respect to the healthy (Aβ+) population, we centered the SVFs by subtracting the average subject-to-Template SVF of the Aβ- group.

The unbiased SVF were then analyzed by following the proposed framework, to show that advanced AD stages are associated with accelerated aging plus a disease specific anatomical pattern. The effectiveness of the disease specific component in encoding information relevant to the pathology was tested by performing two different discriminative analysis on the classification between AD vs healthy, and MCI_{conv} vs MCI_{stable}.

3.1 Estimated virtual aging.

The normal aging modeled for the Aβ- group is shown in Figure 2 (left), and is characterized mainly by the ventricular enlargement and by atrophy in the temporal areas. The estimated virtual age is significantly correlated with the biological one for all the considered groups (minimum Pearson's r for the MCI_{conv} (0.3) and maximum for the MCI_{stable} (0.54), $p < 0.005$) . However, even though the considered groups did not significantly differ for age, the virtual age increases as the clinical condition gets closer to AD. In fact, as shown in Figure 2, Aβ+, MCI_{conv}, and AD are increasingly virtually older when compared to the healthy Aβ- (p-values in the boxes). Interestingly, MCI_{conv} are significantly older than MCI_{stable} (p=0.035), to indicate a possible accelerated aging process induced by the ongoing AD.
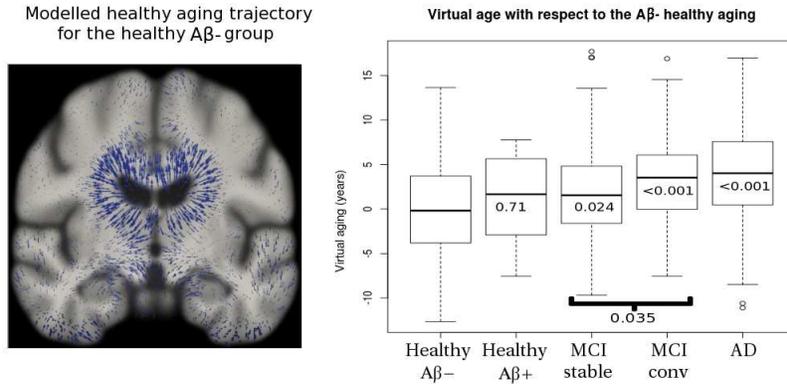

Fig. 2: Left: Normal aging modeled for the group of Aβ- healthy subjects. Right: Average virtual age estimated for the clinical groups with respect to the normal aging. The estimated virtual ages describe statistically significant older brains (standard t-test, p-value in the boxes) with respect to the healthy Aβ- for all the considered groups. Interestingly, MCI converters are "virtually older" than the MCI stables (p < 0.0392).

3.2 Analysis of the specific component.

Figure 3 shows the average specific deformation components ν_k associated to the different groups once centered with respect to the healthy population. The morphological changes specific for the healthy Aβ+ are mild, while the changes specific for the MCI converters are more pronounced and map to the frontal cortex, ventricles, temporal poles, entorhinal cortex and hippocampi. The same pattern is appreciable for the AD patients.
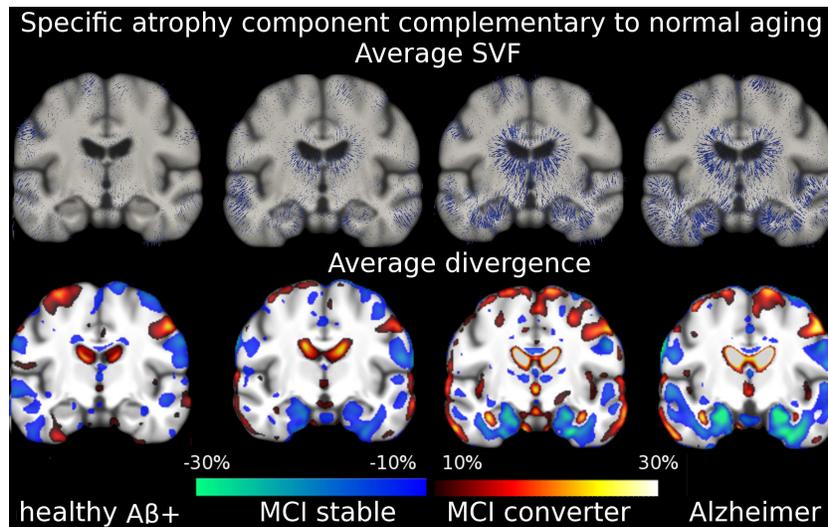

Fig. 3: First row: average specific deformation component not related to normal aging. MCI converters and AD patients show the more pronounced pattern of morphological changes mapping mainly to ventricles, temporal poles, entorhinal cortex and hippocampi. Second row: percentage matter loss measured by the average divergence maps extracted from the specific component.

In Figure 3, second row, we notice that the change in the clinical condition (from Aβ+, to MCI_{conv} and AD) is associated with larger and more intense divergence patterns (i.e. flux across regions). For each anatomical region we can identify the associated location of high positive divergence (growth of the

CSF regions), and the correspondent area of high negative divergence (brain atrophy), which indicate more intense expansion/compression mapping mainly to ventricles, temporal poles and hippocampi.

Figure 4 shows the effect size between the divergence maps of respectively MCI converters vs stable, and AD vs healthy controls. As expected, the effect size between AD and healthy controls is higher than the one between MCI converters and stables, to indicate the larger variability in the MCI group.
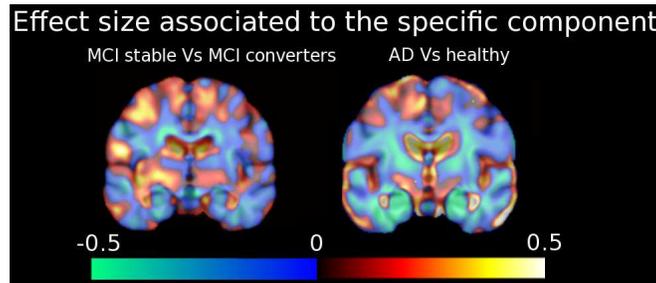

Fig. 4: Effect size associated to the divergence maps of the specific components.

Finally, Table 1 shows the regional and pooled prediction accuracy in the discriminative analysis between AD vs $Ctrls$, and MCI_{conv} vs MCI_{stable}. The fair classification results (91% sensitivity, 84% specificity for AD vs Ctrls, and 67%, 63% for MCI_{conv} vs MCI_{stable}) indicate the ability of the specific pathological component to encode information relevant for the disease condition and the clinical group. The provided predictions are significantly better than those given by pure chance ($p < 0.001$, McNemar's Chi-Square test), and are in line with those available in the literature on the ADNI dataset [3,2].

4   Conclusions.

We proposed a method to decompose the brain atrophy into complementary components: aging and AD specific. These components identify different clinical stages, and are compatible with the hypothesis that points to the positivity to the CSF Aβ42 as a presymptomatic marker of AD in the healthy stages. We showed that more advanced AD stages (from Aβ+ to MCI converters, and finally to AD) are associated to both "virtually older" brains, and to increased specific morphological changes not related to the normal aging.

Different MRI-based indices of brain aging were proposed in the past [6,4]. Our model integrates these approaches into a richer description of the AD process. In fact we showed that AD is *not only* represented by accelerated brain aging, but is also composed by a specific and complementary quote of atrophy. While confirming the results from the other studies, our method points to a completely different conclusion. Since AD is not only an accelerated aging process, the design of *disease specific* modifying drugs which do not have impact on the natural normal aging is then justified.

To conclude, our approach provide new insights which may help the understandings of the AD dynamics, and which might promote the development of novel diagnostic techniques for the early detection of the disease.

References

1. Barnes, C.: Secrets of aging: What does a normally aging brain look like? Biol Rep. 3(22) (2011)
2. Chincarini, A., Bosco, P., Calvini, P., et al.: Local MRI analysis approach in the diagnosis of early and prodromal Alzheimer's disease. NeuroImage 58(2), 469–480 (2011)
3. Cuingnet, R., Gerardin, E., Tessieras, J., Auzias, G., Lehricy, S., Habert, M., Chupin, M., Benali, H., Colliot, O.: Automatic classification of patients with

	AD vs Ctrls				MCI_{conv} vs MCI_{Stable}			
	Sens	Spec	PPV	NPV	Sens	Spec	PPV	NPV
All features	**91**	**84**	**85**	**90**	54	54	54	54
MTL (-)	86	81	85	82	53	51	52	52
MTL (+)	73	77	76	74	57	57	57	57
Hippocampi (-)	77	71	75	73	55	47	51	51
Hippocampi (+)	77	63	73	67	**67**	**63**	**64**	**65**
Ventricles (+)	65	69	68	66	61	43	52	52
Ventricles (-)	68	69	69	68	58	56	57	57
PC (-)	58	59	59	59	58	58	58	58
PC (+)	59	50	54	54	47	74	64	58

Table 1: Regional classification accuracy for the leave-one-out discrimination. The analyzed features are the positive and negative flux (+ and -) of the specific component across the regions of interest.

Alzheimers disease from structural MRI: a comparison of ten methods using the ADNI database. NeuroImage 56(2), 766–781 (2011)

4. Davatzikos, C., Xu, F., An, Y., Fan, Y., Resnik, S.: Longitudinal progression of Alzheimer's-like patterns of atrophy in normal older adults: the SPARE-AD index. Brain 132(8), 2026–2035 (2009)

5. Fjell, A., Walhovd, K., Notestine, C., et al.: Brain atrophy in healthy aging is related to csf levels of Ab1-42. Cereb. Cortex 20-9 (2010)

6. Franke, K., Ziegler, G., Klöppel, S., Gaser, C.: Estimating the age of healthy subjects from T1-weighted MRI scans using kernel methods: Exploring the influence of various parameters. NeuroImage 50(3), 883–892 (2010)

7. Frisoni, G., Fox, N., Jr, C.J., Scheltens, P., Thompson, P.: The clinical use of structural MRI in alzheimer disease. Nat Rev Neurol 6, 67–77 (2010)

8. Jack, C., Knopman, D., Jagust, W., et al.: Hypothetical model of dynamic biomarkers of the Alzheimer's pathological cascade . Lancet Neurol 9(1), 119–128 (2010)

9. Long, X., Liao, W., Liang, D., Qiu, B., Zhang, L.: Healthy aging: An automatic analysis of global and regional morphological alterations of human brain. Acad Radiol. 14 (2012)

10. Lorenzi, M., Ayache, N., Frisoni, G., Pennec, X.: Mapping the effects of $A\beta_{1-42}$ levels on the longitudinal changes in healthy aging: hierarchical modeling based on

stationary velocity fields. In: MICCAI. pp. 663–670. LNCS, Springer (2011)

11. Lorenzi, M., Ayache, N., Pennec, X.: Regional flux analysis of longitudinal atrophy in alzheimer's disease. In: MICCAI. LNCS, Springer (2012)

12. Nelson, P.T., Head, E., Schmitt, F., Davis, P., et al.: Alzheimers disease is not "brain aging": neuropathological, genetic, and epidemiological human studies. Acta Neuropathol. 121(5), 571–587 (2011)

13. Scahill, R., Schott, J., Stevens, J., Rossor, M., Fox, N.: Mapping the evolution of regional atrophy in Alzheimer's disease: unbiased analysis of fluid-registered serial MRI. Proc Natl Acad Sci 99, 4703–4707 (2002)

14. Tosun, D., Schuff, N., Truran-Sacrey, D., et al.: Relations between brain tissue loss, csf biomarkers, and the apoe genetic profile: a longitudinal MRI study. Neurobiol Aging 31-8 (2010)